An integrated deep learning solution for petrophysics, pore pressure, and geomechanics property prediction

Ehsan Zabihi Naeini[1], Sam Green[1], Iestyn Russell-Hughes[1], and Marianne Rauch-Davies[2]

https://doi.org/10.1190/tle38010053.1.

Abstract

In unconventional plays, wells are drilled at an unprecedented rate. This, together with technical challenges in terms of complex stratigraphy, multiple play types, variable rock properties, and various elements of pore pressure, geomechanics, fracturing, and diagenesis, calls for more sophisticated, faster, consistent, and wider ranging analytical tools. Given the scale of the work — i.e., the number of wells — performing classical workflows for petrophysics, pore pressure, and geomechanics prediction can be impractical (if not impossible) due to turnaround considerations. Also such workflows might not use any preexisting regional studies efficiently. In principle, a machine learning approach can mitigate these shortcomings. We show that a supervised deep neural network approach can be an alternative innovative tool for petrophysical, pore pressure, and geomechanics analysis enabling the use of all the previously interpreted data to devise solutions that simultaneously integrate wide-ranging wellbore and wireline logs. Beyond that, a similar approach is taken to predict a certain number of attributes solely from seismically derived properties, which allows one to compute volumetric models. The application of such an algorithm is shown on a Permian case study in which the automatic neural-network-based algorithms achieve reasonable accuracy in a fraction of the time.

Introduction

In unconventional resource plays, pore pressure prediction plays a critical role in the ability to predict areas of high overpressure and fracture behavior for the exploitation of these plays, which are both correlated with production. Traditional pore pressure prediction focuses exclusively on clay-rich shales and assumes that all shales have a porosity/effective stress relationship that can be used to link the mechanical compaction of the rock to the pore pressure via the vertical stress (overburden). Unconventional shales are uplifted and are affected by chemical processes and diagenetic alteration of the elastic properties such that porosity is not typically relatable to effective stress, resulting in a more complex pore pressure prediction workflow.

Shales in unconventional plays also have variable clay content and complex multimineral fractions that require a detailed petrophysical assessment reinforced with rock-physics modeling where needed. For example, changes in total organic content (TOC) have a similar response in elastic properties to changes in porosity. Therefore, any pressure-stress property model for unconventional plays must be supported by clean, petrophysically conditioned elastic logs and accurate multimineral sets calibrated to core data. Having said that, the multimineral petrophysical assessment is a time-consuming process because each well must be assessed individually before being quality checked as part of a multiwell process for consistency.

The Permian Basin, which is a mature hydrocarbon "superbasin" located primarily in west Texas and extending into southeastern New Mexico, has produced more than 39 billion barrels (cumulative) of oil since it began production in the 1920s. The conventional production peak in 1973 of 790 million barrels was surpassed in 2017 with 815 million barrels of oil (IHS, 2018) due to unconventional production. The most astonishing fact of all is that as many as 1 million additional wells might be drilled in the foreseeable future (Nunn et al., 2018). This, together with the Permian's technical challenges in terms of complex stratigraphy, near-surface complications that affect velocity modeling, multiple play types, variable rock properties, and various elements of pore pressure, geomechanics, fracturing, and diagenesis, calls for more sophisticated, faster, consistent, and wider ranging analytical tools. Given the scale of the work — i.e., the number of wells — performing classical workflows is impractical (if not impossible) due to turnaround considerations and also may not use previous regional studies efficiently. These factors are the motivation behind this paper, which presents machine learning as an alternative innovative tool for petrophysical, pore pressure, and geomechanics analysis enabling the use of all available data to devise solutions that simultaneously integrate wide-ranging wellbore and wireline data.

The case study presented here, located in the Delaware Basin of the wider scale Permian Basin, demonstrates the effectiveness of focusing on building integrated petrophysical, pore pressure, and geomechanical models for a selection of key wells. Subsequently, a machine-learning-based approach can be used to produce consistent interpretations for the desired properties. This approach has the advantage that once the algorithm is trained efficiently, it then can be quickly applied to any number of wells within the area of interest. However, sufficient care must be taken to assure the algorithm generalizes to the new cases as part of the training process and to ensure that the workflow incorporates a robust cross-validation strategy.

The following sections discuss the standard approach and the development of a neural network algorithm to predict petrophysical properties, pore pressure, and stress to understand drilling and completion behavior, and ultimately production, better.

Standard unconventional workflows

Multimineral petrophysics. Petrophysical interpretation of unconventional plays can be challenging and time consuming. The mineralogy of these rocks tends to be complex, with a mix of carbonates, siliciclastics, and organic-rich beds. The presence

[1]Ikon Science, London, UK. E-mail: enaeini@ikonscience.com; sgreen@ikonscience.com; irhughes@ikonscience.com.
[2]Devon Energy Corporation, Oklahoma City, Oklahoma, USA. E-mail: marianne.rauch-davies@dvn.com.

of kerogen in the rock will lead to high readings on gamma ray and resistivity, with higher porosity being indicated by logs such as density and sonic. The kerogen effect also must be accounted for in any petrophysical analysis of these plays.

A common approach to petrophysical interpretation of such rock types is the use of a multimineral solver. This allows the petrophysicist to generate a volume of each mineral and fluid deemed present in the rock. A volume of kerogen also can be generated within the model or calculated initially using various methods (Passey et al., 1990; Vernik, 2016) and the resultant volume included as an input into the multimineral solver. The resultant multimineral model often requires parameter adjustment or some log normalization at each well. Another vital part of this workflow is the calibration of results. Traditionally, this is achieved using core data. Core measurements of TOC are used to calibrate the kerogen volume while mineral volumes can be calibrated using X-ray diffraction (XRD) and interpreted porosity adjusted to core porosity. It is often the case that such data are scarce, or nonexistent, which can lead to default regional values being employed in the analysis.

Pore pressure and geomechanics property prediction. The critical assumption underpinning traditional pore pressure prediction is that the variations observed in specific wireline data (P- and S-sonic often expressed as V_P, V_S, density, neutron, and resistivity) vary solely due to changes in porosity and that the porosity is controlled by the pore pressure. Shales in unconventional plays are (or were) at high temperature leading to diagenetic alteration of the mineralogy, are often dramatically uplifted, and have been affected by chemical processes in addition to mechanical compaction such that porosity might not be solely relatable to effective stress. Furthermore, the link between pore pressure and log response can be disrupted further by the presence of organic material (high TOC) and/or free gas in the pore space. Although these challenges are not unique to unconventional plays, they are more likely to be present. An increase in TOC has been shown to significantly lower the magnitudes of velocity and density (Passey et al., 1990). Gas in the pore space has a similar slowing effect on the V_P data. Although the TOC effect has a linear relationship with log response, the gas effect is not as straightforward to correct for due to the nonlinear effect of gas saturation. Slow velocity (either due to TOC or to free gas in the pores) and low density are typically attributed to an increase in pore pressure, as they imply high porosity, so the TOC/gas effect should be removed from log data in order to correctly predict pore pressure.

In spite of these issues, it still can be possible to derive a relationship between wireline data and the pressure magnitude. Ebrom et al. (2003) demonstrated a relationship between V_S and pore pressure that circumvents the effect of gas on the V_P data by modifying the Eaton (1975) pore pressure method with a bespoke exponent. More recently, Zhang and Wieseneck (2011) presented a case study from the Haynesville and Bossier plays in the southern United States where a pseudo-V_P was computed from measured V_S using a calibrated Castagna approach to avoid the slowing effect of gas on measured V_P. This approach was further modified by Couzens-Schultz et al. (2013) who showed that V_S data could be used directly to predict pore pressure in the same unconventional plays. The two recent examples mentioned here used the Bowers (1994) method to develop the pore pressure prediction algorithm.

The execution of geomechanical modeling in unconventional plays is more established and does not suffer from the same prior assumptions (dependence on a porosity-effective stress relationship) that pore pressure analysis does. However, the pore pressure is a critical input into the geomechanical model. Hence, there is a critical dependence on the petrophysical conditioning of the data, as well as the multimineral petrophysics. Rauch-Davies et al. (2018) highlighted that geomechanical behavior cannot be robustly predicted without a reliable estimate of the pore pressure.

Deep learning

A neural network is a powerful machine learning tool characterized by its neurons and the corresponding weights, biases, and activation functions. When a neural network has multiple fully connected layers, it is known as a deep neural network or a deep learning mechanism. Deep neural networks can be implemented to perform either classification or regression tasks. The activations function imposes nonlinearity and differentiates deep neural networks from linear regression methods.

In this study, the designed neural network has the structure shown in Figure 1. Because the objective is to predict various continuous properties (e.g., petrophysics, pore pressure, and geomechanics), the network performs a regression task. The activation function is a rectified linear unit, known as ReLU. A ReLU is a nonlinear function allowing back propagation of errors across multiple layers. The cost function in this study is the root-mean-square error between the predicted and the training values minimized using a gradient descent method.

To quality control (QC) the performance of the deep neural network, a robust cross-validation strategy was implemented, consisting of two parts. First, 20% of the training data were set aside to track the minimization performance during the training and avoid overfitting. Second, a number of wells were set aside for blind testing after the training was complete. In what follows, we

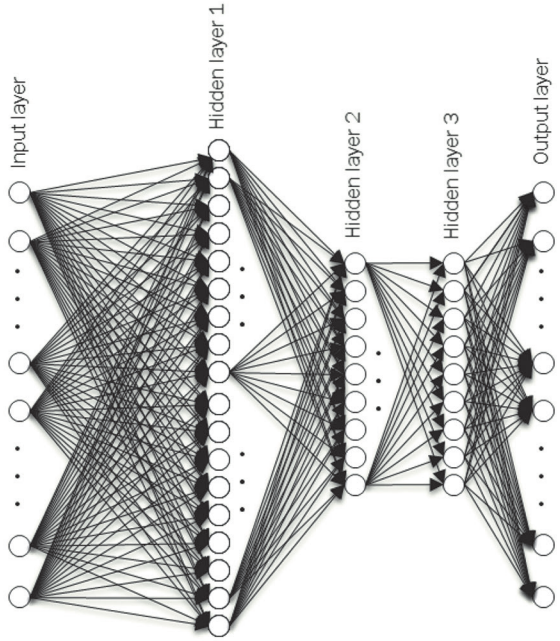

Figure 1. A schematic display of the neural network implemented in this study. Each neuron is characterized by its weights, bias, and ReLU activation function.

show the properties predicted via the deep neural network in the blind wells and compare the precision against the manually interpreted data where available. Furthermore, the implemented workflow was integrated such that some of the outputs from the predicted petrophysics logs (e.g., volume of shale and kerogen) were fed to the subsequent pore pressure and geomechanics networks.

We then take a further step by predicting the same properties using the seismic data over the same area as the wells. Given that one can obtain compressional and shear velocities and density (namely, V_P, V_S, and rho) from isotropic prestack amplitude-variation-with-offset inversion (e.g., facies-based method proposed as discussed in Kemper and Gunning, 2014, and Zabihi Naeini and Exley, 2017), a separate network was trained to predict pore pressure, volume of kerogen, and geomechanical properties from the logs at the training wells. Then the network was applied to the corresponding V_P, V_S, and rho from seismic inversion at the wells. After quality checking the outcomes at the wells, shown in the following sections, the network was applied to the entire volume. The result of our study for both workflows mentioned earlier is shown on a Permian case study to follow.

Case study: Delaware Basin, Permian

Preparing training data for an integrated deep-learning-based prediction

1) Petrophysics. Well data used in this study were drawn from a previously executed extensive petrophysical analysis. As part of that study, approximately 1500 wells were evaluated, with abundant core data used for calibration of the final petrophysical results. This case study is based on a smaller subset of this data set. Figure 2 shows the location of the 13 training wells and four blind test wells and also shows the seismic survey encompassing the training wells and two of the blind test wells. The two other blind test wells are located approximately 50 km to the southeast of the seismic survey to test the applicability of using the neural network away from the initial training well data set.

As part of conditioning the data, logs from various vintages required careful QC — i.e., log editing was performed to remove anomalous data, and log normalization and synthetic generation were also performed to create a consistent data set. Volume of clay was calculated from a combination of a number of methods, including gamma ray and neutron density. The resultant volume was calibrated to core XRD data. TOC was estimated using the Passey method (Passey et al., 1990) and tied to core. Volume of kerogen was then calculated from TOC. The porosity, saturation, and other volumes (quartz, limestone, and dolomite) were then generated using the workflows described earlier. Additional data, such as nuclear magnetic resonance, gamma ray spectroscopy, reservoir properties, and chemistry were incorporated where possible. A final QC to ensure multiwell consistency was performed. This formed the basis of training data and blind wells QC for the performance of deep-learning-based predictions.

2) Pore pressure and geomechanics. The pore pressure model was constructed using direct measurements of pore pressure taken from either dynamic fracture initiation tests (DFIT), drill-stem tests (DST), or by an influx as interpreted from the drilling history. The pressure data, expressed as vertical effective stress (VES; vertical stress minus pore pressure) were crossplotted against the compressional velocity (V_P) shifted by 5000 ft/s following the approach of Bowers (1994). Each of these data points was then assigned a quality flag based on the lithology it was taken in and the confidence in the wireline data at the same depth (Figure 3). The primary concern was the role of cement producing fast velocities which would have produced incorrect V_P-VES models. Secondary concerns were TOC and in-situ gas, but neither of

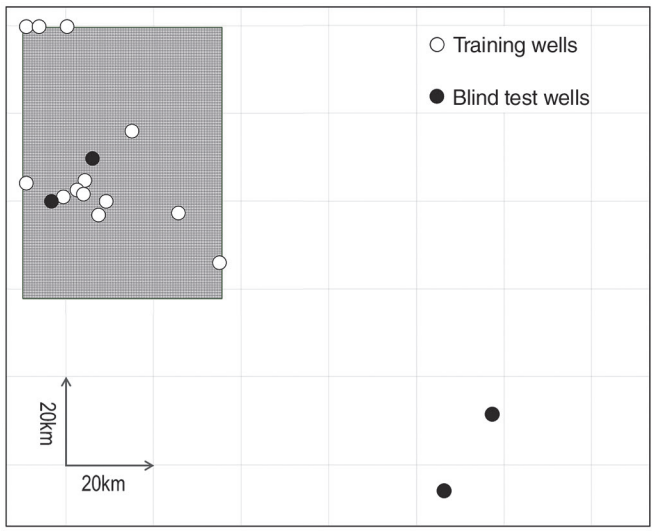

Figure 2. Base map showing location of the training wells within the seismic survey area and the location of the blind test wells. The initial blind test wells are located within the survey, close to the training data, but two more blind test wells, approximately 50 km away, were chosen to highlight the effectiveness of the derived machine learning algorithm.

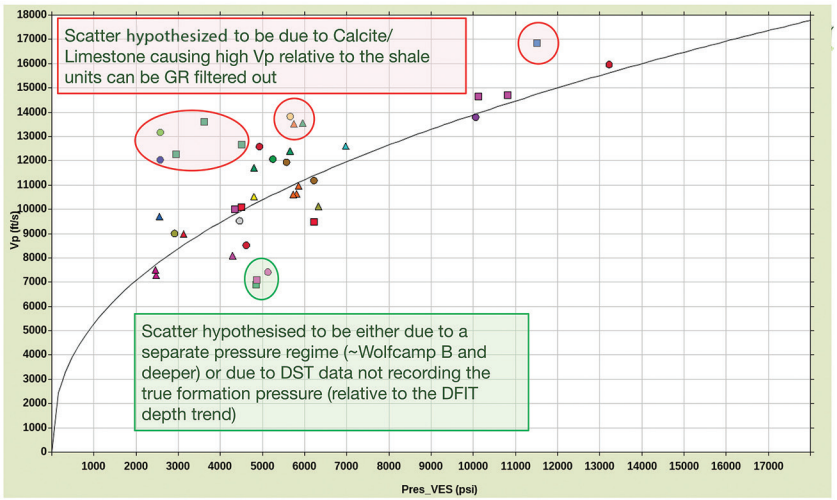

Figure 3. Velocity-effective stress crossplot showing a range of direct pressure data (DFIT, DST, Kicks) against wireline V_P. A power law relationship following Bowers (1994) is shown, and anomalous data are highlighted and annotated.

these was a major concern within the sand-rich intervals (but remain a source of uncertainty within the shale-rich units).

The geomechanical analysis commenced with an interpretation of the image logs. Observations of drilling-induced tensile fractures were noted. A 1D analytical geomechanical model was then constructed using the poroelastic equations (Thiercelin and Plumb, 1994) and the elastic properties calculated from the well logs using core data to constrain the dynamic to static conversion. The regional strain parameters were calibrated to the minimum horizontal stress magnitude determined from DFIT measurements and to the maximum horizontal stress magnitude by solving the circumferential (hoop) stress around a vertical borehole and matching the predicted tensile failure to the occurrence (and nonoccurrence) of drilling-induced tensile fractures observed in the image logs (e.g., a blind test well from the geomechanical analysis in Figure 4). The calibrated model was then applied using the upscaled elastic log data to verify that the expected resolution of the property volumes to be determined by the seismic inversion would be sufficient to predict the DFIT closure pressure and tensile failure observed in the image logs.

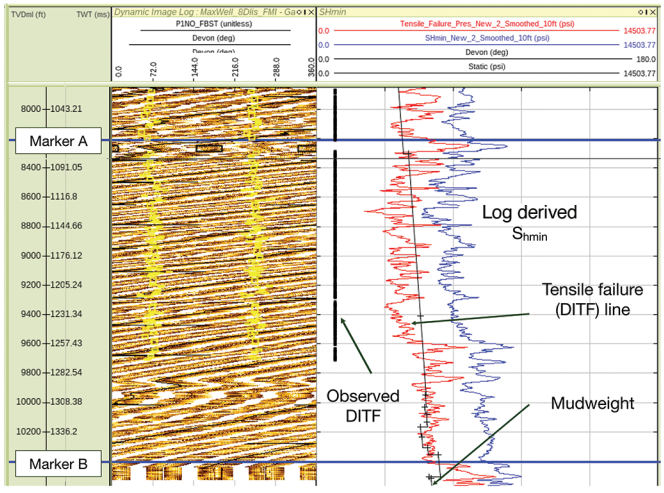

Figure 4. Example of the outputted tensile failure line (red curve) compared to the mudweight (thin black line) for a blind test well. The image log (left-hand track) records tensile failure of the wellbore down to approximately 9700 ft, as shown in the log track by the thick black line, which matches the behavior predicted from the geomechanical model — i.e., tensile failure curve is less than the mudweight.

3) Seismic-based property prediction. The seismic inversion used a facies-based Bayesian prestack approach (Kemper and Gunning, 2014). There were two key advantages to applying this approach in this case study. First, the inclusion of facies in the inversion process removed the requirement for a conventional low-frequency model. This ensured that the distribution of laterally discontinuous units was defined only by the seismic reflectivity and not biased by any interpolation assumptions. Second, the inversion approach was calibrated using a set of facies-dependent elastic property trends, rather than a single set of trends for the whole inversion window (Payne and Meyer, 2017). Therefore, the predicted elastic impedance properties could be expected to honor the rock-physics relationships observed in the well-log data with greater fidelity. This is important when considering the subsequent geologic characterization and geomechanical analysis using the property volumes. Given the inverted V_P, V_S, and density using this method, the neural network (trained to predict the desired properties using well logs) was then applied to the entire seismic volume.

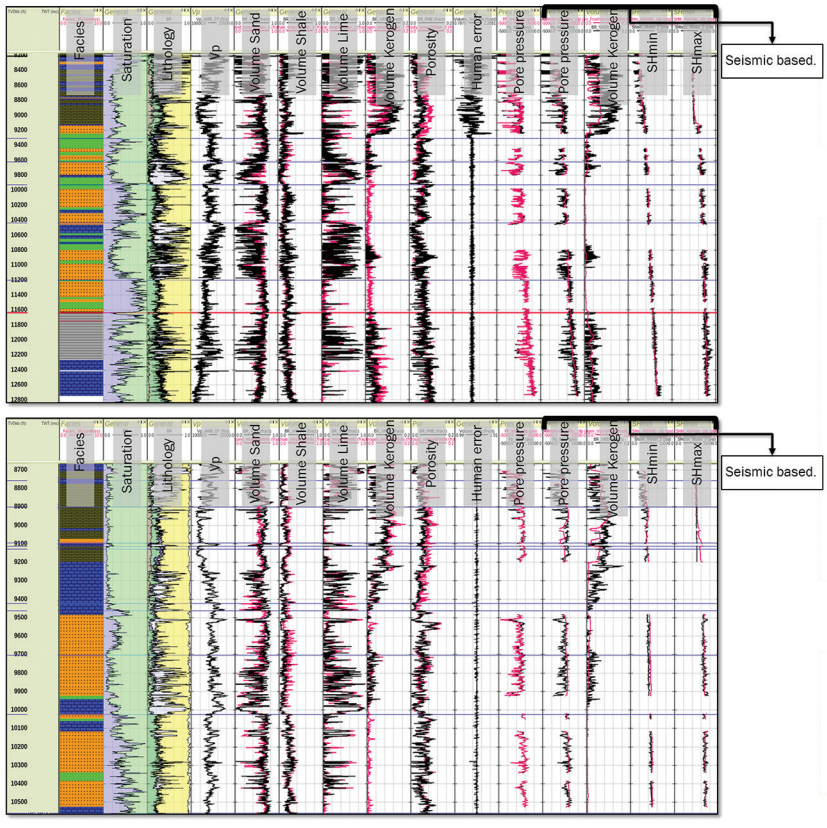

Figure 5. Both blind test wells within the seismic survey area. Black data are the well-based petrophysics and rock-physics (pore pressure and geomechanics) model-based curves. The red curves are the product generated from the machine learning algorithm. At nearly all depths and for all log types, there is an excellent match between the well-based and machine-learning-based results.

Deep learning predictions

We implemented three main neural networks all with similar structure as mentioned in the "Deep learning" section. The reason was that each of these networks had a different objective, and the outputs from one were the inputs for the other.

Step 1: The first network was to predict petrophysical properties. The inputs for training were compressional velocity, gamma ray, density, resistivity, and neutron logs. The network was trained to predict volumes of shale, sand, dolomite, calcite, kerogen, and porosity simultaneously. Figure 5 shows the predicted properties (red

curves) versus manually interpreted logs (black curves) in the corresponding log tracks. It can be observed that the predicted properties demonstrate a reasonable accuracy when compared to the manually interpreted logs. With this QC in mind, the key benefit from the deep learning method is that the network can be applied in other wells in the area with an extremely fast turnaround as the application to new wells takes only seconds. This was examined on one of the wells outside the seismic volume, approximately 50 km away, as shown in Figure 6.

Step 2: Given an initial neural network to predict the petrophysical properties, the second neural network was then designed to predict pore pressure. In this case, the inputs were compressional and shear velocity, density, resistivity, neutron logs as well as porosity, volume of shale, and volume of kerogen predictions from the previous step. The result is shown in the "pore pressure" track in Figure 5. Again the proximity to the classic manual interpretation is evident. Furthermore, the predictions were done on a well outside the seismic volume as shown in Figure 6. One could argue that the reason for such a good prediction is the relatively straightforward rock-physics relationships between V_P, rho, and pore pressure. Still, it is rather appealing that the network captures such behavior. This is shown in the crossplot in Figure 7. The crossplot clearly shows that even with a rather simple rock-physics model, shown with two solid black curves relating to specific lithologic packages, care has to be taken to avoid underfitting. (A similar argument applies for overfitting.) The final fit shows that the neural network does a reasonable job to capture both rock-physics models.

All the QC steps, i.e., blind wells and crossplots, help one to make the right decision in justifying the performance of neural networks in these applications. Such QC steps become more important for more complex regimes (i.e., neural networks must not be treated as a black box with a calculate button). For example, there is a mismatch between the manually interpreted volume curves for lime and sand and the neural network predicted values for the same curves in Figure 6 (approximate depth 10,000 ft). There are two possible reasons for this — either the manual interpretation benefits from additional data (core, composite log, photoelectric absorption factor log) that the neural network does not include, or the manual interpretation has a subjective bias in it that the objective neural network does not. In both cases, lessons are learned that either the network would benefit from additional input data or that the manual interpretations may not be as uniform as originally thought. An example of the latter case can be seen in the blind well in Figure 5 (top) in which the slight inconsistency between the machine-learning-based prediction and manually interpreted porosity and volume of kerogen (at around 8500 ft depth) is due to the error that must have occurred in the manual interpretation workflow (see "human error" track that shows deviation from a total sum of 1 for the total mineral volumes).

Step 3: This part of the study focused on predicting various properties of interest, in this case pore pressure, S_{hmin}, S_{Hmax}, and volume of kerogen, based on only compressional and shear

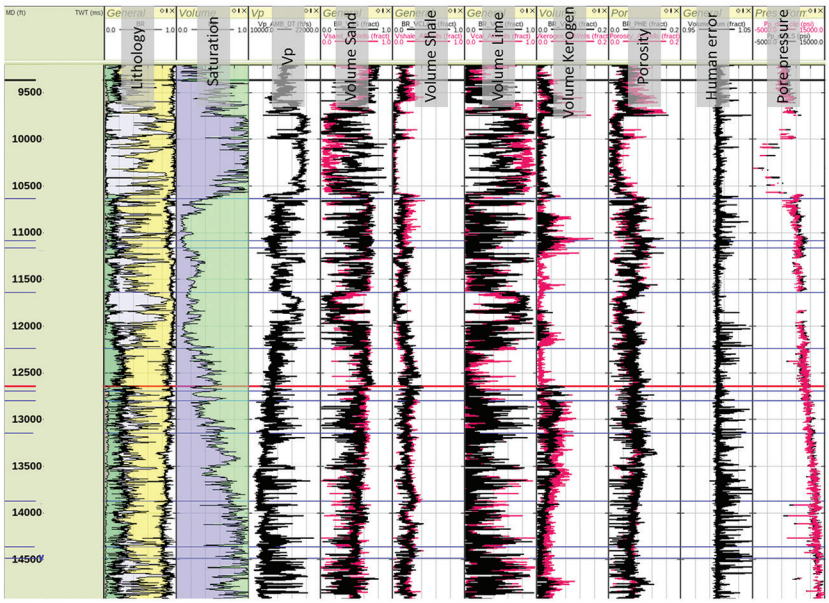

Figure 6. First blind test well outside the seismic survey. Despite the well being located approximately 50 km from the training wells, there is an excellent match between the well-based and machine-learning-based results at most depths. There is a mismatch in the upper section where the machine learning algorithm predicts higher lime/lower sand content relative to the well curves.

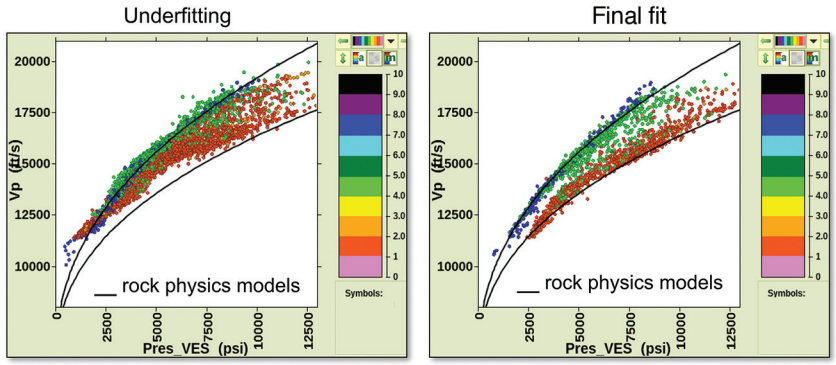

Figure 7. Velocity-effective stress crossplots showing the well-based pore pressure (rock physics) models in black and the results of the machine learning algorithm for the training wells. The color scheme related to the facies within the wells: 1-3 = Leonard, 4-6 = Bone Springs, and 7-9 = Wolfcamp (see Figure 9 for more details). The right-hand plot shows the importance of correctly defining the number of iterations of the model to correctly fit the data. In the left-hand plot, where too little iteration was made, the data are biased to the upper rock-physics model and, hence, underfit to the correct rock-physics model for the shallow lithologies.

velocity and density logs. Designing a network in such manner allows one to not only predict these properties at wells with limited available logs but also be able to predict based on inverted elastic properties from seismic amplitudes. An example of the former is shown in Figure 8, which is a well outside the seismic volume where direct measurements of pore pressure and S_{hmin} were available from a single DFIT taken in the well. The well-based predictions appear to match the DFIT values providing validation for the neural network. Also the seismic-based predictions on the two wells inside the seismic volume are shown in the last four tracks on both panels in Figure 5 using the same neural network.

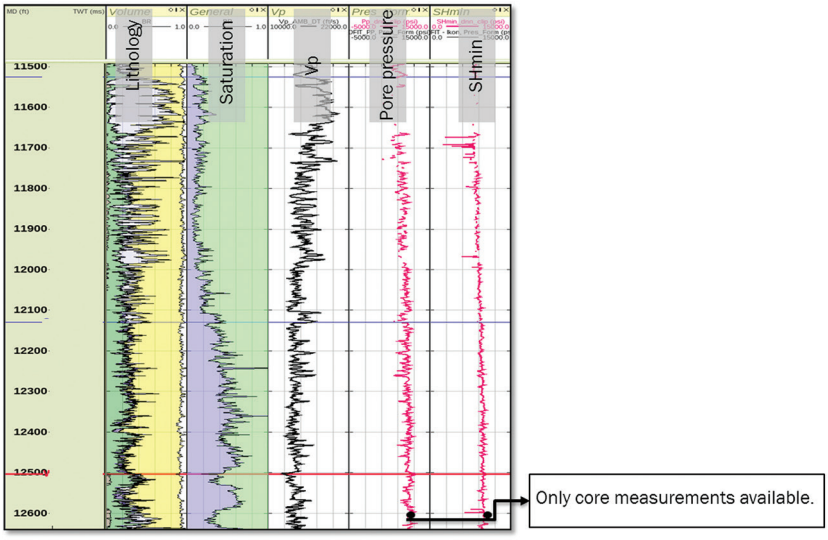

Figure 8. Second blind test well outside the seismic survey. In this well, there were limited petrophysics, so the machine learning algorithm was modified to be based on only V_P, V_S, and rho, which also provided the framework to upscale the approach into the seismic domain. There is an excellent match between the test results from a DFIT taken at the base of the well (black circles) and machine-learning-based results shown by the red curves.

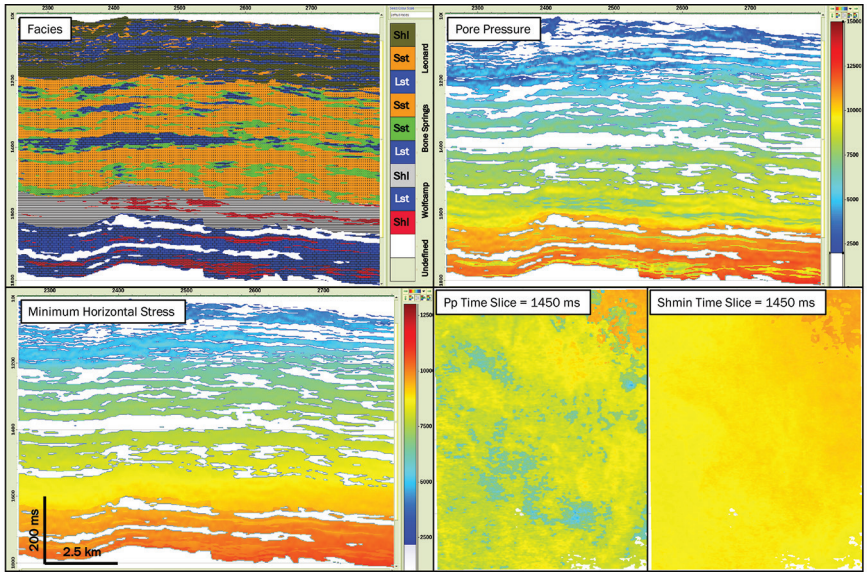

Figure 9. Composite image showing the results of the machine learning algorithm when applied to the seismic inversion data. The input data were the facies (upper left) and volumes of V_P, V_S, and rho (not shown). The outputted pore pressure (cross section = upper right; time slice = left-hand bottom right) and minimum horizontal stress (cross section = lower left; time slice = right-hand bottom right).

Because seismic resolution is limited by the frequency bandwidth, the predicted properties demonstrate a deficiency in resolution when compared to manually interpreted logs in depth. Nonetheless, one can observe that there is a good overall match where the predicted logs capture the main behavior — i.e., high magnitudes versus low magnitudes. Upon the completion of these QCs at the blind wells, it is straightforward to apply the network to the entire volume of V_P, V_S, and density values derived from seismic inversion. This leads to volumetric models of pore pressure and geomechanical properties (S_{hmin} and S_{Hmax}). These are shown in Figure 9. These volumetric models could be used to perform a sweet spot analysis, for example, based on multiple cut-offs for pore pressure, S_{hmin}, and volume of kerogen.

Testing the results against the geomechanical data also proves the accuracy of the pore pressure volumes as these are inputs into the geomechanical models. With that in mind, the values of the 3D property models are evident when blind wells that have drilled long lateral sections are used to compare production, using 60 days of cumulative oil production in barrels normalized to the length of the lateral, with the pore pressure volume. The upper panel in Figure 10 shows a horizontal section from a well drilled within the Leonard interval; plotted along the well path is the gas log recorded during drilling. The hot colors (red/yellow) indicate higher pore pressure within the interval, and the presence of elevated gas is clearly linked to areas of higher pore pressure in both the vertical and horizontal sections. This relationship is clearly shown along the horizontal section as the majority of the well penetrates dominantly low pressure (greens/blues), and the gas level is low until the high-pressure zone at the toe of the lateral is penetrated at which point the gas level increases significantly.

Furthermore, if the 60-day normalized cumulative oil production values are quoted for wells plotted within the same variably overpressured interval, then the role of high pore pressure in mapping out more productive zones is clear (lower panels in Figure 10). The well (A) that is consistently located within the high-pressure zone records cumulative oil production of more than 61,000 barrels of oil, whereas the well that misses the highest pressures show returns of approximately 30% (18,000 barrels) over the same timescale.

Conclusions

After discussing the standard workflows, a supervised deep neural network approach was introduced as an alternative innovative tool for petrophysical, pore pressure, and geomechanics analysis enabling the use of all the previously collected and interpreted data to devise solutions which simultaneously integrate wide-ranging wellbore and wireline logs. Furthermore, an algorithm was developed to predict a certain number of attributes solely from seismically derived properties, namely V_P, V_S, and density. The application of these algorithms on various blind wells from a Permian case study, both within and outside the seismic survey, show a reasonable accuracy when compared to manually interpreted counterparts, but they were obtained in a fraction of the time. The volumetric pore pressure model was also correlated consistently with cumulative production values from blind long horizontal wells. Of course, one can argue that the underlying rock-physics behavior in the case study is an ideal scenario with a relatively straightforward pore pressure system; however, the results show a promising outlook for the application of deep learning in integrated studies such as those shown in this paper. TLE

Acknowledgments

The authors would like to thank Devon Energy Corporation for permission to publish the case study. The authors are also grateful to Jeremy Meyer for contribution and review. Seismic data were provided courtesy of Fairfield Geotechnologies.

Data and materials availability

Data associated with this research are confidential and cannot be released.

Corresponding author: enaeini@ikonscience.com

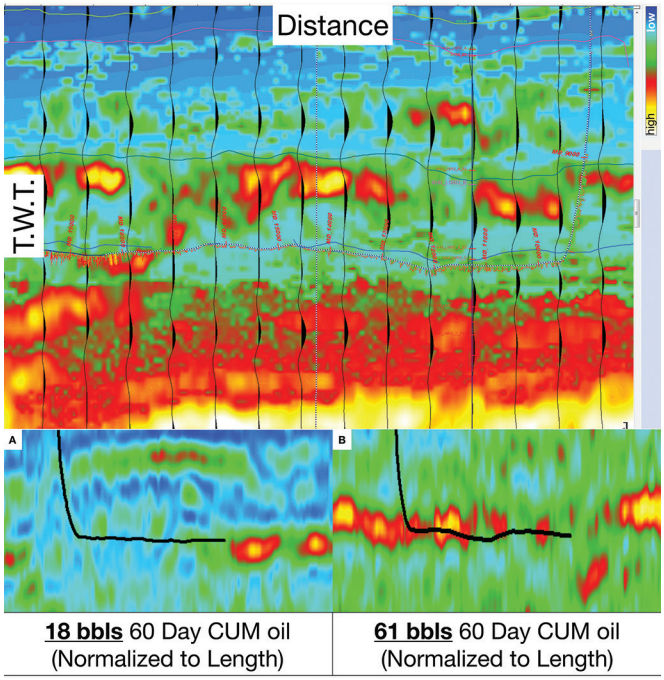

Figure 10. The cross section shows the variation in predicted pore pressure (hot colors = high pressure) within the Leonard shale interval. In the upper image, a wellbore is plotted with the lateral section intercepting both higher and lower pressure sections. A gas log (thin curve along well trajectory) demonstrates that where the pore pressure is high — e.g., the toe of the lateral section — the well experiences higher gas levels while drilling. Conversely, where pore pressure is lower — e.g., the middle of the lateral section — very little gas response is recorded. The two cross sections at the base of the figure show examples of lateral sections from producing wells drilled within the Leonard shale interval. Where the lateral sections are located within the high-pressure zones (red), the 60-day cumulative oil production values, normalized to the length of the lateral, are approximately 61,000 barrels as opposed to 18,000 barrels (approximately 30%) where the wells penetrate lower pressure shales.

References

Bowers, G. L., 1994, Pore pressure estimation from velocity data accounting for overpressure mechanisms besides undercompaction: Annual Technical Conference and Exhibition, IADC/SPE, 515–530.

Couzens-Schultz, B. A., A. Axon, K. Azbel, K. S. Hansen, M. Haugland, R. Sarker, B. Tichelaar, et al., 2013, Pore pressure prediction in unconventional resources: International Petroleum Technology Conference, https://doi.org/10.2523/IPTC-16849-MS.

Eaton, B. A., 1975, The equation for geopressure prediction from well logs: 50th Annual Fall Meeting, SPE, https://doi.org/10.2118/5544-MS.

Ebrom, D., P. Heppard, M. Mueller, and L. Thomsen, 2003, Pore pressure prediction from S-wave, C-wave, and P-wave velocities: 73rd Annual International Meeting, SEG, Expanded Abstracts, 1370–1373, https://doi.org/10.1190/1.1817543.

IHS, 2018, https://ihsmarkit.com/solutions/permian-basin.html, accessed 29 August 2018.

Kemper, M., and J. Gunning, 2014, Joint impedance and facies inversion — Seismic inversion redefined: First Break, **32**, no. 9, 89–95.

Nunn, J., D. Scolman, and G. Winters, 2018, Introduction to this special section: The Permian Basin: The Leading Edge, **37**, no. 3, 170–170, https://doi.org/10.1190/tle37030170.1.

Passey, Q. R., S. Creaney, J. B. Kulla, F. J. Moretti, and J. D. Stroud, 1990, A practical model for organic richness from porosity and resistivity logs: AAPG Bulletin, **74**, no. 12, 1777–1794.

Payne, S., and J. Meyer, 2017, Using seismic inversion to predict geomechanical well behavior: A case study from the Permian Basin: Proceedings of the 5th Unconventional Resources Technology Conference, https://doi.org/10.15530/URTEC-2017-2665754.

Rauch-Davies, M., B. Schmicker, S. W. Smith, S. Green, and J. J. Meyer, 2018, Predicting pore-pressure from on-shore seismic data in the Delaware Basin: Proceedings of the 6th Unconventional Resources Technology Conference, https://doi.org/10.15530/urtec-2018-2888832.

Thiercelin, M. J., and R. A. Plumb, 1994, Core-based prediction of lithologic stress contrasts in east Texas formations: SPE Formation Evaluation, **9**, no. 4, 251–258, https://doi.org/10.2118/21847-PA.

Vernik, L., 2016, Seismic petrophysics in quantitative interpretation: SEG, https://doi.org/10.1190/1.9781560803256.

Zabihi Naeini, E., and R. Exley, 2017, Quantitative interpretation using facies-based seismic inversion: Interpretation, **5**, no. 3, SL1–SL8, https://doi.org/10.1190/INT-2016-0178.1.

Zhang, J., and J. Wieseneck, 2011, Challenges and surprises of abnormal pore pressures in the shale gas formations: Annual Technical Conference and Exhibition, SPE, https://doi.org/10.2118/145964-ms.